Materials and Design 60 (2014) 510–519

Contents lists available at ScienceDirect

Materials and Design

journal homepage: www.elsevier.com/locate/matdes

Three-point bending of sandwich beams with aluminum foam-filled corrugated cores

L.L. Yan [a,b], B. Han [a], B. Yu [a], C.Q. Chen [c], Q.C. Zhang [a,*], T.J. Lu [a,*]

[a] State Key Laboratory for Mechanical Structure Strength and Vibration, Xi'an Jiaotong University, Xi'an 710049, PR China
[b] College of Science, Air Force Engineering University, Xi'an 710051, PR China
[c] Department of Engineering Mechanics, CNMM, Tsinghua University, Beijing 100084, PR China

ARTICLE INFO

Article history:
Received 27 December 2013
Accepted 4 April 2014
Available online 13 April 2014

Keywords:
Sandwich beam
Corrugated core
Three-point bending
Failure modes

ABSTRACT

Sandwich panels having metallic corrugated cores had distinctly different attributes from those having metal foam cores, the former with high specific stiffness/strength and the latter with superior specific energy absorption capacity. To explore the attribute diversity, all-metallic hybrid-cored sandwich constructions with aluminum foam blocks inserted into the interstices of steel corrugated plates were fabricated and tested under three-point bending. Analytical predictions of the bending stiffness, initial failure load, peak load, and failure modes were obtained and compared with those measured. Good agreement between analysis and experiment was achieved. Failure maps were also constructed to reveal the mechanisms of initial failure. Foam insertions altered not only the failure mode of the corrugated sandwich but also increased dramatically its bending resistance. All-metallic sandwich constructions with foam-filled corrugated cores hold great potential as novel lightweight structural materials for a wide range of structural and crushing/impulsive loading applications.

1. Introduction

High performance lightweight sandwich constructions require the cores to have high stiffness and strength as well as energy absorption capacities. It was recently envisioned that this may be achieved by combining stochastic foams with periodic lattice trusses [1]. The concept was simple and straightforward. Sandwiches with lattice truss cores were widely applied as primary loading structures due to high stiffness/strength to weight ratio [2–7], yet they usually softened rapidly once the peak load was reached due to node failure and/or core buckling. With a long plateau region after initial failure was initiated, sandwich structures with metallic foam cores were attractive for energy absorption applications [8,9], yet their stiffness and peak strength were limited by a multitude of initial geometric defects induced during processing [10,11]. To mingle the advantageous attributes of foams and lattices, a variety of approaches had been attempted, including combing polymer foams with metallic lattices [12–15], polymer foams with polymer lattices [16–18], and metallic foams with metallic lattices [1].

The hybrid lattice/foam-cored sandwich panels thus constructed were so far studied mainly under out-of-plane uniform compression (quasi-static and dynamic), both experimentally and theoretically. The beneficial effect of foam filling was found to be strongly dependent upon the type of combination. For instance, combining relatively weak polymer foams with metallic lattices led only to limited enhancement of stiffness/strength and energy absorption [13]. Built upon the existing studies, the focus of the present investigation was placed upon examining the three-point bending performance of metallic corrugated sandwiches filled with aluminum foams using a combined experimental and analytical approach.

Using finite element (FE) simulations, Vaziri et al. [13] found rather limited effect of inserting polymeric foams (Divinycell) into the interstices of metallic sandwich panels with corrugated cores, which was attributed to the insufficient lateral support provided by the filling foam to the core members against buckling. Subsequently, also using sandwich panels having corrugated cores as the prototype, Yan et al. [1] replaced the filling polymeric foam with close-celled aluminum foams and demonstrated, both experimentally and numerically, that the compressive strength and energy absorption capacity of the corrugated sandwich panel were much greater than the sum of those of an empty sandwich panel and the aluminum foam alone.

Besides out-of-plane uniform compression, sandwich panels in engineering applications were commonly subjected to other types of load such as three-point bending. The bending responses of sandwich structures with a variety of lightweight cellular cores

* Corresponding authors. Tel.: +86 29 8266 5600; fax: +86 29 8266 5937.
E-mail addresses: zqc111999@mail.xjtu.edu.cn (Q.C. Zhang), tjlu@mail.xjtu.edu.cn (T.J. Lu).

http://dx.doi.org/10.1016/j.matdes.2014.04.014
0261-3069/

had been extensively studied, including lattice truss cores (corrugated plates [18–21], Y-frames [21], honeycombs [15,22,23] and pyramidal trusses [24]) and metallic [25–27] and polymeric foam cores [28]. The effect of dynamic loading was also examined [23,29–31]. Nonetheless, the bending performance (including stiffness, failure load and failure mechanisms) of all-metallic sandwich panels with aluminum foam-filled cores was yet to be investigated. In fact, sandwich panels with either periodic lattice or stochastic foam cores were known to have relatively low resistance to shear/bending. How this might be mended by combing metallic lattices with aluminum foams to make use of their respective attributes as the core for sandwich constructions was the main focus of the present study.

The paper was organized as follows. Sandwich beams with aluminum foam-filled corrugated cores were fabricated and tested under quasi-static three-point bending. For comparison, empty (unfilled) corrugated sandwich beams were also tested. Analytical predictions of the bending stiffness, initial failure load and peak load were obtained and compared with those experimentally measured. Failure maps were constructed to reveal the failure mechanisms underlying the enhanced bending performance of the hybrid-cored sandwich structures. Finally, the performance of the foam-filled sandwich was compared with several competitive designs.

2. Experimental measurement

2.1. Fabrication of test samples

Fig. 1 illustrated schematically the fabrication procedures for sandwich beams having empty and aluminum foam-filled corrugated cores. Both the face sheets and core web (*i.e.*, strut) of the sandwich were made of 304 stainless steel (density $\rho_s = 7900$ kg/m^3). Commercial closed-cell aluminum alloy foam with density of $\rho_f = 540$ kg/m^3 was selected as the filling material [32]. To this end, triangular foam prisms having the same shape of the interstices of the corrugated plates were cut by electro-discharge machining (EDM) from aluminum foam sheets. The triangular foam prisms were then inserted into the interstices and fixed with epoxy glue. Before assembling, surface cleaning was applied to both the empty sandwich beam and the foam prisms. The foam-filled sandwich was hold at 25 °C for 4 h, heated up to 80 °C for 2 h, and then cooled to ambient temperature.

2.2. Three-point bending test

Quasi-static three-point bending tests (Fig. 2) were conducted on MTS-880 materials test system, with fixed loading rate of 0.5 mm/min according to ASTM: C393 and ASTM: D7249 for beam flexure test of sandwich constructions. Both long and short sandwich beams were tested, as shown in Fig. 3, the former with a total length of 312 mm (*i.e.*, 9 unit cells) and the latter with 180 mm (*i.e.*, 5 unit cells), and the loading span L between the supports were 242 and 112 mm, respectively (Fig. 2). The force and displacement of the specimens were measured by the loading cell of the test machine. Unloading was performed to measure the bending stiffness instead of the loading curve. A rig was manufactured for the test to ensure the loading condition was simplified three-point bending. The support and the head of the loading device were steel cylinders of 10 mm in diameter, each attached to a flat pedestal with width of 10 mm to avoid force concentration. To study the deformation and failure modes of the sandwich beams, digital deforming images of each specimen were acquired by video camera.

As listed in Table 1, the sandwich specimens used for the present three-point bending tests had fixed width of $b = 40$ mm, fixed strut thickness of $t = 0.41$ mm, fixed inclination angle of $\theta = 45°$, and fixed core height of $h_c = 17$ mm. Further, closed-cell aluminum

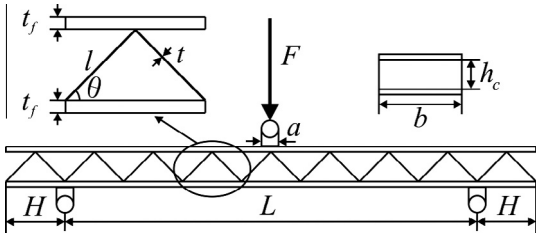

Fig. 2. Schematic of corrugated sandwich beam subjected to three-point bending.

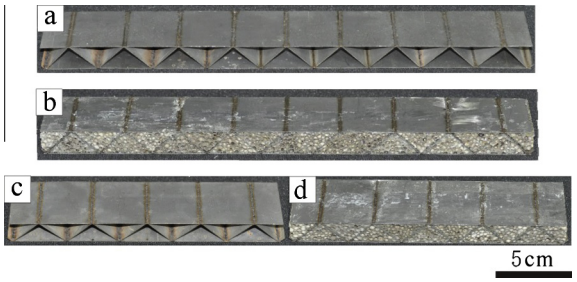

Fig. 3. Typical as-fabricated empty and aluminum foam-filled sandwich beams with corrugated cores. Long beam: (a) empty; and (b) filled. Short beam: (c) empty; and (d) filled.

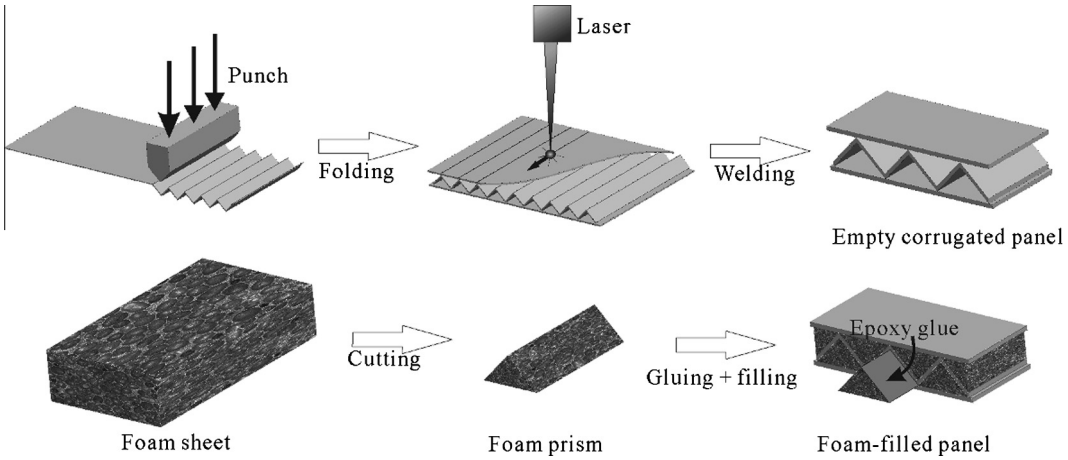

Fig. 1. Fabrication process of corrugated sandwich beams with unfilled and aluminum foam-filled cores [1].

Table 1
Parameters of empty and aluminum foam-filled corrugated sandwich specimens for three-point bending test.

Specimen	A	B	C	D	E	a	b	c	d	e
Core type	Foam-filled					Empty				
Span L (mm)	242	242	112	112	112	242	242	112	112	112
t_f (mm)	0.82	0.41	2.0	0.82	0.41	0.82	0.41	2.0	0.82	0.41
$\bar{\rho}$	0.18	0.14	0.27	0.18	0.14	0.12	0.08	0.22	0.12	0.08

foam with fixed density of $\rho_f = 540$ kg/m^3 and averaged cell size of ~2 mm was chosen as the filling material.

With the densities of steel and aluminum foam denoted separately by ρ_s and ρ_f, the average density of the foam-filled corrugated core ρ_c was defined as:

$$\rho_c = v_s\rho_s + \rho_f(1 - v_s) \tag{1}$$

where v_s was the volume proportion of the core occupied by steel:

$$v_s = 2t/l\cos 2\theta \tag{2}$$

Here, θ was the inclination angle, t was the strut thickness, and l was the strut length. For empty sandwich, $\rho_f = 0$; for foam-cored sandwich, $v_s = 0$.

With the facesheets of the sandwich beam considered, the total average relative density of the sandwich beam $\bar{\rho} = \rho/\rho_s$ may be expressed as:

$$\bar{\rho} = \frac{2t_f + h_c\rho_c/\rho_s}{2t_f + h_c} \tag{3}$$

where ρ was the total average density of the sandwich beam, t_f was thickness of the steel facesheet, and h_c was the core height. The thickness of core web $t = 0.41$ mm, core height $t_f = 17$ mm and core web inclination angle $t_f = 45°$ were fixed for each specimen. Close-celled aluminum foam with density of $t_f = 540$ kg/m^3 was used as the filling material. The facesheets and core webs were both made of 304 stainless steel (density $t_f = 7900$ kg/m^3). The top and bottom facesheets had identical thickness t_f. Accordingly, the average density of the empty and foam-filled corrugated cores was fixed at $\rho_c = 253$ and 776 kg/m^3, respectively. The total relative densities of the sandwich beams investigated in the present study were listed in Table 1.

3. Theoretical analysis of foam-filled sandwich beams under three-point bending

As previously mentioned, whilst the deformation, failure and optimal design of empty corrugated sandwich beams have been investigated extensively, no such study was carried out for foam-filled corrugated sandwiches subjected to three-point bending, either experimentally or theoretically. To address the deficiency, this section focused on theoretical analysis of the foam-filled sandwiches in three-point bending. The results were used in the next section to compare with the present experimental measurements. Numerical results obtained with finite element (FE) simulations and optimal design for three-point bending loaded foam-filled sandwiches were reported in an companion study [33].

3.1. Sandwich stiffness

For an empty or foam-filled corrugated sandwich beam loaded in 3-point bending, the total deflection δ at its mid-point may be given as the sum of the deflections due to bending of the face sheets and shear of the core [34]:

$$\delta = \frac{FL^3}{48(EI)_{eq}} + \frac{FL}{4(GA)_{eq}} \tag{4}$$

where $(EI)_{eq}$ and $(GA)_{eq}$ were the equivalent flexural rigidity and shear rigidity, respectively, that may be expressed as:

$$(EI)_{eq} = \frac{Ebt_fd^2}{2} + \frac{Ebt_f^3}{6} + \frac{C_{22}^H bc^3}{12} \tag{5}$$

$$(GA)_{eq} = \frac{bd^2}{c}C_{44}^H \approx bcC_{44}^H \tag{6}$$

Here, C_{22}^H was the in-plane elastic modulus of the core in the 2-direction, and C_{44}^H was the out-of-plane shear modulus of the core in the 2–3 direction. By using the homogenization method, these two elastic constants may be obtained as [33]:

$$C_{22}^H = \frac{E}{(1-v^2)}\left(\frac{t}{l}\right)\frac{\cos^3\theta}{\sin\theta} + \frac{E}{(1-v^2)}\left(\frac{t}{l}\right)^3\sin\theta\cos\theta + \frac{2\kappa E}{(1-v^2)}\left(\frac{t}{l}\right)\frac{\cos\theta}{\sin\theta} + (1-v_s)C_{11}^f \tag{7}$$

$$C_{44}^H = \frac{E}{(1-v^2)}\left(\frac{t}{l}\right)\sin\theta\cos\theta + \frac{1}{4}\frac{E}{(1-v^2)}\left(\frac{t}{l}\right)^3\left(\frac{\sin^3\theta}{\cos\theta} + \frac{\cos^3\theta}{\sin\theta} - \sin\theta\cos\theta\right) - \frac{E}{(1-v^2)}\left(\frac{t}{l}\right)\psi + (1-v_s)C_{66}^f \tag{8}$$

$$C_{11}^f = \frac{(1-v_f)E_f}{(1-2v_f)(1+v_f)} \tag{9}$$

$$C_{66}^f = \frac{E_f}{2(1+v_f)} \tag{10}$$

$$\kappa = \frac{v}{E}\left(\sin^2\theta C_{11}^f + \cos^2\theta C_{12}^f\right), \quad \psi = \frac{4v}{E}C_{66}^f\sin\theta\cos\theta \tag{11}$$

In the foregoing expressions, E and v denoted the elastic modulus and Poison ratio of the parent material of the face sheets and core webs, E_f and v_f referred to the elastic modulus and elastic Poison ratio of the filling foam, and v_s was the volume proportion of the core occupied by the steel defined by Eq. (2).

3.2. Initial failure

For foam-filled corrugated sandwich beams subjected to three-point bending, four main modes of collapse were identified: (1) face yielding, (2) face elastic/plastic wrinkling, (3) indentation and (4) core shear, which were confirmed by systematic FE simulations [33]. Typical failure modes corresponding to indentation and core shear were illustrated schematically in Figs. 4 and 5, respectively. In the following, plane strain assumed so that for the core webs, the effective Young's modulus $\widehat{E}_s = E_s/(1-v^2)$ and the yield stress $\hat{\sigma}_y = 2\sigma_y/\sqrt{3}$. Similarly, for the filling foam, the effective Young's modulus $\widehat{E}_f = E_f/(1-v_f^2)$, the plateau stress $\hat{\sigma}_{plateau} = 2\sigma_{plateau}/\sqrt{3}$, and the shear strength $\hat{\tau}_{plateau} = \hat{\sigma}_{plateau}/2$.

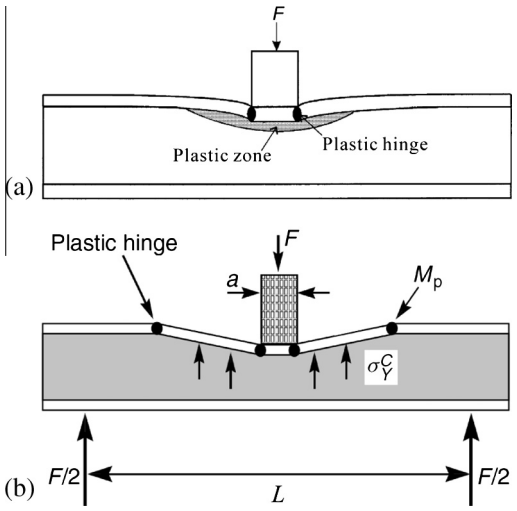

Fig. 4. Schematic of sandwich beam with core indentation collapse mode at: (a) initiation of indention; and (b) limit load for indentation [3,25].

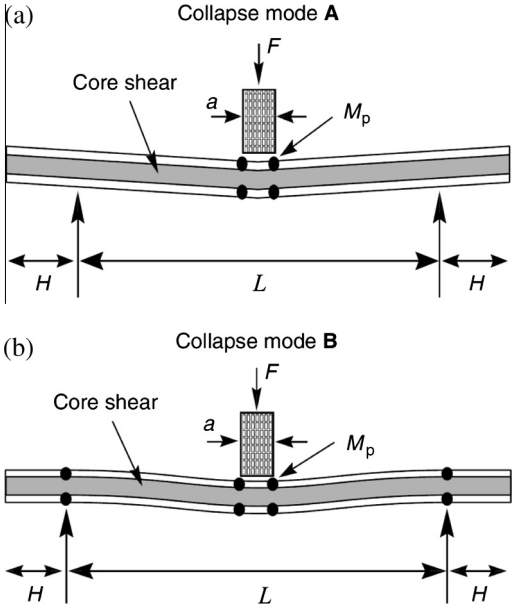

Fig. 5. Schematics of sandwich beam with core shear collapse mode: (a) Mode A; and (b) Mode B [3].

Under three-point bending, when failure was initiated in the foam-filled sandwich, relevant formulae governing the four different modes were summarized as follows.

(1) Face yielding

$$F_{fy} = \frac{4bt_f(c+t_f)}{L}\hat{\sigma}_y \tag{12}$$

(2) Face elastic wrinkling

$$F_{fw} = \frac{4btd}{L}\sigma_f^w \tag{13}$$

where σ_f^w was the wrinkling stress of the face sheet, given by:

$$\sigma_f^w = \sqrt{\frac{\widehat{E}_s\widehat{E}_{foam}}{3}\left(\frac{t_f}{c}\right)} \tag{14}$$

(3) Indentation

$$F_{ind} = \sqrt{2}bt_f\sqrt{\hat{\sigma}_y\Sigma_{33}^{cY}} + ab\Sigma_{33}^{cY} \tag{15}$$

where Σ_{33}^{cY} was the compressive stress of the core in 3-direction, and σ_{cr} is the failure stress of core web [35]:

$$\Sigma_{33}^{cY} = \left[\lambda\sin^2\theta + (1-v_s)\frac{\widehat{E}_{foam}}{\widehat{E}_s\sin^2\theta}\right]\sigma_{cr} \tag{16}$$

$$\sigma_{cr} = \begin{cases} \sqrt{\frac{\widehat{E}_s\widehat{E}_{foam}}{3\cos\theta}\left(\frac{t}{c}\right)}, & \text{if } \sigma_{cr} \leqslant \hat{\sigma}_y \quad \text{core web buckling} \\ \hat{\sigma}_y, & \text{otherwise} \quad \text{core web yielding} \end{cases} \tag{17}$$

(4) Core shear

$$\text{Mode A(Fig. 5a)}: F_A = \frac{2bt_f^2}{l}\hat{\sigma}_y + 2bc\Sigma_{23}^{cY}\left(1+\frac{2H}{l}\right) \tag{18}$$

$$\text{Mode B (Fig. 5b)}: F_B = \frac{4bt_f^2}{l}\hat{\sigma}_y + 2bc\Sigma_{23}^{cY} \tag{19}$$

where Σ_{23}^{cY} was the shear stress of the core in the 2–3 direction, given by:

$$\Sigma_{23}^{cY} = \left[\frac{v_s}{2}\sin(2\theta) + \frac{(1-v_s)E_{foam}}{(1+\upsilon_f)\widehat{E}_s\sin(2\theta)}\right]\sigma_{cr} \tag{20}$$

For the present three-point tests, the overhang (H, see Fig. 3) was large enough that only Mode B of core shear (Fig. 5b) was possible. Further, since the foam used in this paper is stiff enough, buckling of the core web cannot occur as a kind of collapse mode in transverse bending. Only yielding of the core web was considered here, whether in the mode of indentation or core shear.

3.3. Limit load

When failure was initiated in the foam-filled sandwich, the foam insertions remained elastic so that the sandwich could continuously bear the load until the foam yielded. Hence, to predict the limit load corresponding to core shear or indentation failure mode, the compressive and shear stresses of the core should be modified as:

$$\Sigma_{33}^{cY} = v_s\sin^2\theta\hat{\sigma}_y + (1-v_s)\hat{\sigma}_{plateau} \tag{21}$$

$$\Sigma_{23}^{cY} = \frac{v_s}{2}\sin(2\theta)\hat{\sigma}_y + (1-v_s)\hat{\tau}_{plateau} \tag{22}$$

Also, to determine the limit load corresponding to face sheet failure modes, the contribution of the tensile yielding of the core in bending should also be considered, as:

$$\Sigma_{22}^{cY} = v_s\cos^2\theta\hat{\sigma}_y + (1-v_s)\hat{\sigma}_{plateau} \tag{23}$$

(1) Face yielding

The limit load for face sheet yielding was given by:

$$F_f = \frac{4bt_f(c+t_f)}{l}\hat{\sigma}_y + \frac{bc^2}{L}\Sigma_{22}^{cy} \tag{24}$$

(2) Face plastic wrinkling

With the strain hardening effect of the face sheet considered, the limit load for face plastic wrinkling may be expressed as:

$$F_f = \frac{4bt_f(c+t_f)}{l}\sigma_f^w + \frac{bc^2}{L}\Sigma_{22}^{cy} \tag{25}$$

Here, different from existing analysis, σ_f^w was expressed in terms of the plastic wrinkling stress as:

$$\sigma_f^w = \sqrt{\frac{E_e\widehat{E}_{foam}}{3}\left(\frac{t_f}{c}\right)} \tag{26}$$

where the efficient modulus E_e for plastic wrinkling was given by [36]:

$$E_e = \frac{1/E_t + (1-2\nu)/(3E_s)}{3/(4E_t) + (1-2\nu)/E_s} E_t \tag{27}$$

(3) Indentation

As shown in Fig. 5(b), two more plastic hinges in the upper face sheet should be considered. Correspondingly, the limit load of indentation should be modified as:

$$F_{ind} = 2bt_f \sqrt{\sigma_f^y \Sigma_{33}^{cY}} + ab\Sigma_{33}^{cY} \tag{28}$$

(4) Core shear

$$F_B = \frac{4bt_f^2}{l}\hat{\sigma}_y + 2bc\Sigma_{23}^{cY} \tag{29}$$

More details of the theoretical analysis were presented in Han et al. [33]. The validity of the present formulae for both initiation failure load and limit load was checked in the next section against experimental measurements. These formulae were also employed in Section 5 to construct the failure mechanism maps.

4. Results and discussion

In this section, the three-point bending responses of sandwich beams with foam-filled corrugated cores were compared with those of empty core sandwiches. The experimentally measured force versus displacement curves as well as failure modes were also compared with analytical predictions. Whilst typical responses of both long and short sandwich beams were presented in the following sections, Table 2 summarized the experimental and theoretical results for all the specimens considered in the present study, including stiffness, load at initial failure, peak load, and failure mode(s).

The bending stiffness $\widetilde{E}$ and failure load $\widetilde{F}$ were normalized by $\bar{\rho}$ as:

$$\widetilde{E} = \frac{F/\delta}{\bar{\rho}} \tag{30}$$

$$\widetilde{F} = \frac{F}{\sigma_Y b L \bar{\rho}} \tag{31}$$

where σ_Y was the yield strength of 304 stainless steel, b and L was the width and loading span of the sandwich beam, and $\bar{\rho}$ was the total average relative density of the sandwich beam defined by Eq. (3).

4.1. Responses of long sandwich beam

The long sandwich beams had a fixed loading span of L = 242 mm. A typical loading force versus displacement curve of the long sandwich beam with foam-filled corrugated core (Specimen B, Table 1) was plotted in Fig. 6(a). For comparison, the corresponding curve of the empty sandwich beam (Specimen b, Table 1) was also plotted. Optical images of the specimen at selected loading points as marked on the force displacement curve were presented in Fig. 6(b), revealing the initiation and evolution of failure as the loading was continuously increased.

It was seen from Fig. 6(a) that filling of aluminum foam into the interstices of corrugated core changed dramatically the force versus displacement curve of the sandwich beam, enhancing significantly its load-bearing capacity. In the case of the empty sandwich, after the initial linear elastic stage, the loading force increased nonlinearly, peaking at 325.2 N as the displacement was increased to 0.49 mm; subsequently, the loading force dropped immediately due to face sheet wrinkling. In sharp contrast, the curve of the foam-filled sandwich exhibited both linear and stable nonlinear stages before the peak load of 1920.7 N was reached at a displacement of 2.68 mm. Subsequently, wrinkling of the top face sheet due to local debonding (failure of epoxy glue; see Fig. 6(a) and (b)) occurred in the central portion of the specimen (adjacent to the load platen), causing rapid decrease of the loading force. However, different to the empty sandwich, beyond the peak load, the foam-filled sandwich still had a load-bearing capacity of 1500 N, much higher than even the peak load (325.2 N) of the empty one. In addition to the significantly elevated peak load, filling with aluminum foam also led to dramatically increased bending stiffness, from 908.2 N/mm to 2067.5 N/mm.

Whilst plastic face wrinkling (P-FW) along with interfacial debonding dominated the failure of the foam-filled sandwich beam, elastic face wrinkling (E-FW) was the main failure mode for the empty one as indicated in Fig. 6(a). In other words, under the present three-point bending, foam filing not only increased dramatically the mechanical properties of the sandwich such as bending stiffness and peak loading force, but also altered the failure mode. Similar conclusions were reached under quasi-static out-of-plane compression [1]. Further, Fig. 6(b) also revealed that no breakage of welding joint occurred in either the empty or foam-filled

Table 2
Summary of experimental measured (Exp.) and analytically predicted (Anal.) results.

Specimen	Stiffness $\widetilde{E}$ (N mm^{-1})		Initial failure			Failure at peak load			Observed failure mode
	Anal.	Exp.	Predicted Failure mode	Failure load ($\widetilde{F}\times 10^3$)		Failure mode	Failure load ($\widetilde{F}\times 10^3$)		
				Anal.	Exp.		Anal.	Exp.	
Filled									
A	19.64	19.38	FY	6.40	6.23	P-FW	14.58	11.75	P-FW
B	13.78	12.95	FY	4.02	4.09	P-FW	7.50	6.75	P-FW
C	161.94	78.78	ID	37.23	31.75	FY	51.82	47.12	FY+DB
D	138.46	113.11	FY	29.89	37.03	P-FW	78.73	71.06	P-FW
E	111.5	93.97	FY	29.96	30.89	P-FW	48.70	47.32	P-FW
Empty									
a	26.29	20.61	E-FW	4.37	3.07	E-FW	4.37	3.07	E-FW
b	21.18	11.35	E-FW	1.70	2.0	E-FW	1.71	2.0	E-FW
c	142.71	53.80	E-CB	15.40	15.56	E-CB	15.40	15.56	E-CB
d	162.22	84.33	E-FW	24.52	25.12	E-FW	24.52	25.12	E-CB
			E-CB	26.69		E-CB	26.69		
e	157.42	25.55	E-FW	13.61	11.88	E-FW	13.61	11.88	E-FW

*Observed failure modes were labeled as: Face yielding (FY); Plastic face wrinkling (P-FW); Elastic face wrinkling (E-FW); Elastic core buckling (E-CB); Indentation (ID); Debonding (DB).

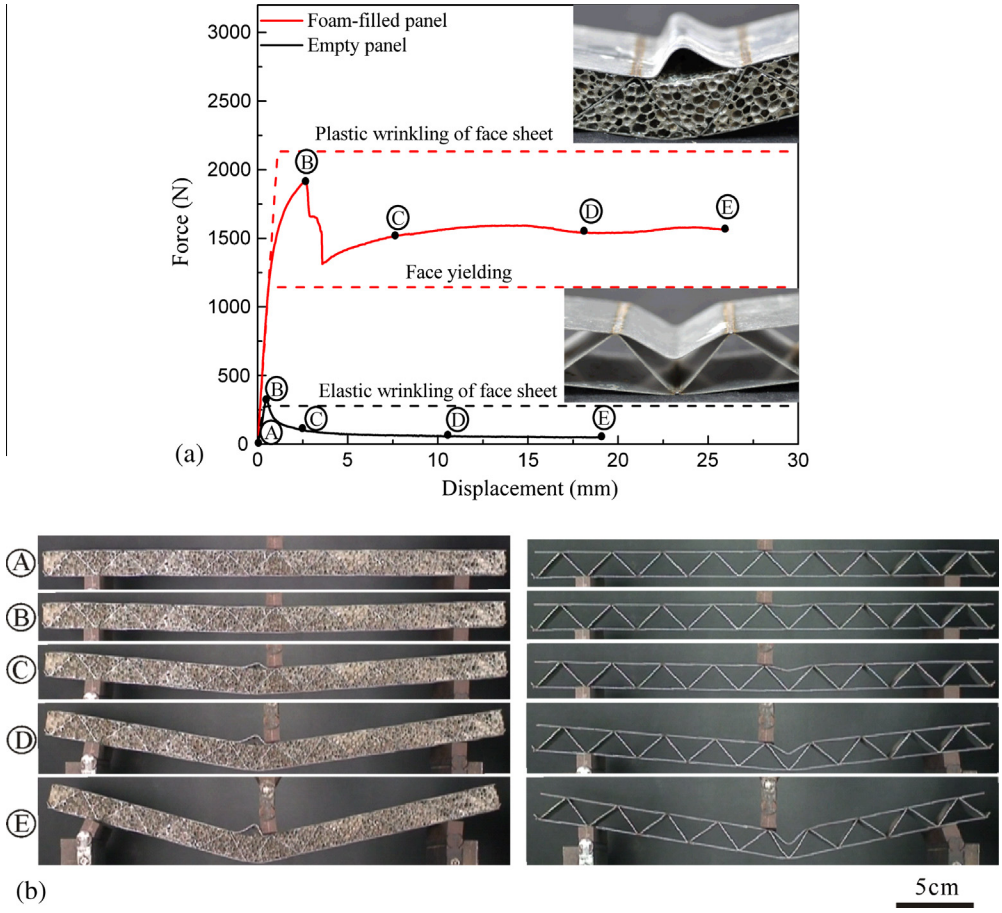

Fig. 6. Transverse bending behavior of empty and foam-filled sandwich beams with corrugated cores (long specimens b and B, with L = 242 mm; Table 1): (a) force versus displacement curve; and (b) photographs illustrating the deformation history and evolution of failure at selected points marked in (a).

sandwich during the whole test: only overall beam bending and face sheet failure were observed.

Analytical predictions for the bending stiffness, initial failure load and peak load of the foam-filled sandwich beam were presented in Fig. 6(a); see also Table 2. The predicted stiffness agreed well with that measured experimentally, having a deviation of only 6%. With face yielding assumed, the predicted initial failure load of 1144.4 N was close to that measured, 1163 N. Consequently, initial failure of the specimen was caused by face yielding. The peak load calculated by assuming plastic face wrinkling was 2133.1 N, slightly higher than the measured one, 1920.7 N. The over prediction was attributed to local debonding between aluminum foam and face sheet that was not considered in analytical modeling.

For the empty sandwich beam, based on experimental observations (Fig. 6), elastic face wrinkling was assumed to calculate both the initial failure load and the peak load. As seen from Fig. 6 and Table 2 the analytical predictions of stiffness, initial failure load and peak load were considerably higher than those measured experimentally. This was largely due to the effects of initial geometric imperfections induced during the fabrication stage in the empty sandwich specimens. In contrast, due to the support of foam insertions, the foam-filled sandwiches were insensitive to initial geometric imperfections, as confirmed by finite element simulations [1]. This was another advantage of the foam-filled sandwiches over the empty ones.

4.2. Responses of short sandwich beam

The short sandwich beams tested had a fixed loading span of L = 112 mm, in comparison with L = 242 mm for long beams. For both empty and foam-filled short sandwich beams (Specimens e and E, Table 1) subjected to three-point bending, Fig. 7(a) compared the experimental measurements with those predicted analytically. Optical images of the specimens at different loading stages as marked in Fig. 7(a) were presented in Fig. 7(b). Further comparison was provided in Table 2.

Similar to long sandwich beams, the resistance of the short ones to bending was increased dramatically due to foam filling. For instance, the peak load was increased nearly 7 times from 894.1 N to 6232.2 N whilst the displacement at which the peak load was reached was increased almost 10 times from 0.38 mm to 3.75 mm. Subsequently, the load was nearly halved due to plastic face wrinkling (P-FW) as well as local debonding before it increased gradually to a constant level of about 4000 N. Upon reaching the peak load, the long plateau stage exhibited by the sandwich as shown in Fig. 7(a) was attributed to the considerable stabling effect of foam filling against strut buckling. In contrast, in the absence of foam filing, upon reaching the peak load where the failure of elastic face wrinkling (E-FW) occurred, the load bearing capacity of the sandwich was continuously reduced with increasing bending deformation. The initiation and evolution of the different failure modes associated with the empty and foam-filled sandwich beams were shown in Fig. 7(b). Here, similar to long sandwich beams, the alteration of failure mode due to foam filling was the main cause underlying the elevated bending resistance of the foam-filled sandwich.

Besides experimental results, Fig. 7(a) also presented the analytically predicted stiffness, initial failure load and peak load. The results of Fig. 7(a) and Table 2 suggested that, in contrast with the foam-filled beam, the stiffness of the empty beam was

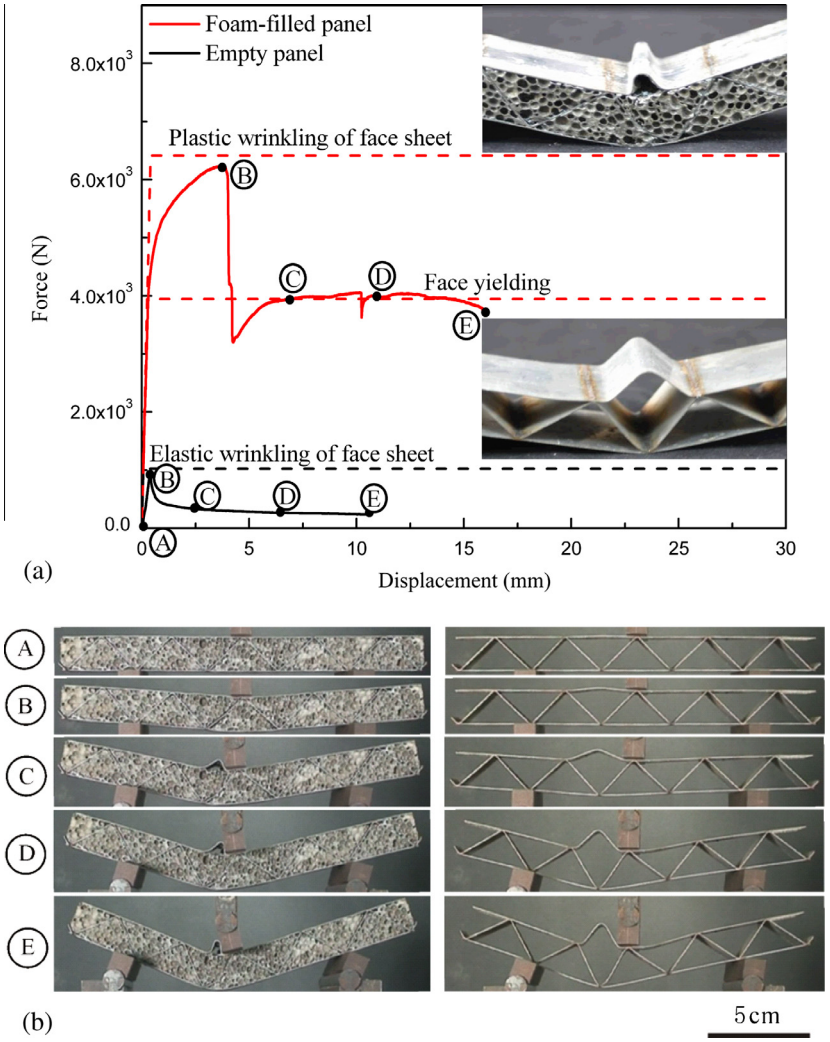

Fig. 7. Transverse bending behavior of empty and foam-filled sandwich beams with corrugated cores (short specimens e and E, with L = 112 mm; Table 1): (a) force versus displacement curve; and (b) photographs illustrating the deformation history and evolution of failure at selected points marked in (a).

significantly over-predicted. This was because the empty beam was sensitive to initial geometric imperfections yet the present model did not consider the effects of imperfections. By assuming that the initial failure and failure at peak load for the empty sandwich were dominated by elastic face wrinkling, the predicted failure load was 1024.5 N, slightly higher than the experimental measured 894.1 N. For the foam-filled sandwich, the predicted initial failure load with face yielding assumed agreed well with that measured. Based on the observed failure mode (Fig. 7(b)), the peak load predicted with the mode of plastic face wrinkling also had good agreement with experimental measurement, indicating the creditability of the present analytical predictions.

4.3. Summary and comparisons

The performances of selected long and short sandwich beams subjected to three-point bending were discussed in previous sections. For comparison, the experimental results and analytical predictions for all the specimens were summarized in Table 2. In general, the analytical predictions agreed well with the experimental measurements and observations. The most notable features were as follows: (i) For empty sandwiches, elastic face wrinkling (E-FW) and elastic core buckling (E-CB) were the dominant failure mechanisms, whereas for foam-filled sandwiches plastic face wrinkling (P-FW) became the dominate failure mode. (ii) As a result of the altered failure mechanisms due to foam filling normalized initial failure load and peak load all increased dramatically for each sandwich beam. (iii) The face sheet thickness t_f and the loading span L had significant effects on the bending performance of both foam-filled and empty sandwiches; as either t_f or L was increased, both the bending stiffness and failure load were increased dramatically. (iv) For empty sandwich beams, the predicted bending stiffness was considerably smaller than that measured. This was attributed to the initial geometric imperfections induced during processing as the thickness of core web was relatively thin (t = 0.41 mm). (v) At large deflections, local debonding between the face sheet and the filling foam only occurred in specimen C of foam-filled sandwiches, for which debonding became the dominate peak failure mode.

5. Failure maps of initiation failure

Formulas for predicting the initial failure modes of sandwich beams with both empty and foam-filled cores were adopted in this section to construct the failure maps so that the dominant initial failure mechanisms may be revealed. To this end, the ratio of core height c to loading span L was selected the abscissas of the failure map, while the ratio of face thickness t_f to core height c was the

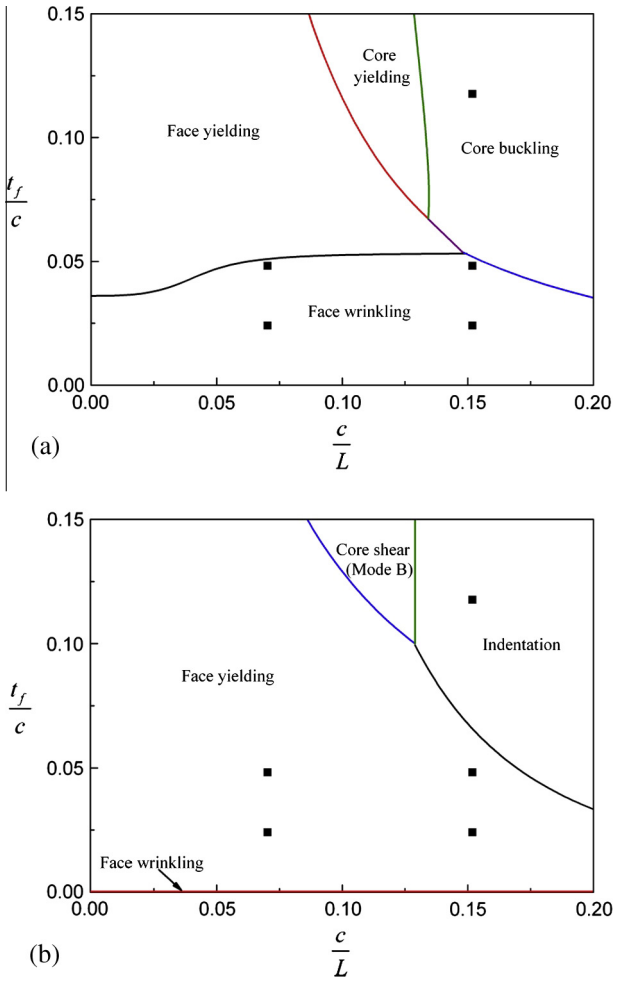

Fig. 8. Initial failure map for sandwich beams with (a) empty and (b) aluminum foam-filled corrugated cores subjected to three-point bending. Face wrinkling and core buckling were all elastic failure, t_f was face sheet thickness, L was loading span, and c = 17 mm was core height.

ordinate axis. In the present study, the core height was fixed at c = 17 mm. Relevant materials properties used to develop the failure maps were given as follows: for face sheets and core webs made of 304 stainless steel, the Young's modulus E = 210 GPa, Poisson ratio υ = 0.3, and yielding stress σ_y = 210 MPa; whilst for closed-cell aluminum foams, the Young's modulus E_f = 2.6 GPa, Poisson ratio υ_f = 0.3, and plateau stress $\sigma_{plateau}$ = 14.5 MPa.

Figs. 8(a) and (b) presented the predicted maps of initial failure for empty and foam-filled sandwich beams, respectively. The experimental data were added to the map, shown as solid squares. Note that, for foam-filled sandwiches, the predicted face wrinkling line (red[1] thick line in Fig. 8(a)) was very close to the abscissas, for face wrinkling occurred only when the face sheet was sufficiently thin. Therefore, due to the remarkable strengthening effect of foam filling, the failure mode of elastic face wrinkling was unlikely to occur in foam-filled sandwiches [1]. Further, as shown in Section 3.2, two different failure modes of core sheer were expected to occur. However, for the large overhang of the specimens studied here, only mode B was considered and plotted in Fig. 8(b).

As shown in Fig. 8(a), for empty sandwich beams considered in the present study, failure was dominated by elastic face wrinkling (E-FW) and elastic core buckling (E-CB), which agreed well with experimental observations as shown in Table 2. Note that for specimen d of Table 2, the analytically predicted failure load with the failure mode of either E-FW or E-CB was close to that experimentally measured. Consequently, in the failure map of Fig. 8(a), specimen d was located in between the E-FW and E-CB regimes. For relatively long sandwich beams, it may be expected that face yielding would occur when the face sheet thickness was increased.

For the foam-filled sandwich beams, the dominant failure mode was face yielding (FY) rather than elastic face wrinkling (E-FW) and elastic core buckling (E-CB) for the empty ones; see Fig. 8(b). Although the observed failure mode was plastic face wrinkling (P-FW) at large deflections as discussed in the previous sections, the FY failure mode was the cause of initial failure. For specimen C, however, the predicted failure mode of indentation agreed well with experimental observation (Fig. 8(b) and Table 2), suggesting that its initial failure mode was ID even though local interfacial debonding occurred later at large deflections.

6. Comparison with competing core designs

Figs. 9(a) and (b) compared separately the measured out-of-plane peak compressive strength σ_{33}^{Peak} and specific energy absorption (SEA) W_m of foam-filled sandwich with several competing core designs, including empty corrugated cores, diamond cores [37], square-honeycomb cores [38] and pyramidal truss cores [39,40]. Except for the aluminum foam filling, the facesheets and the competing cores were all made of 304 stainless.

The energy absorption capacities of different sandwich core designs were typically characterized using the area of the

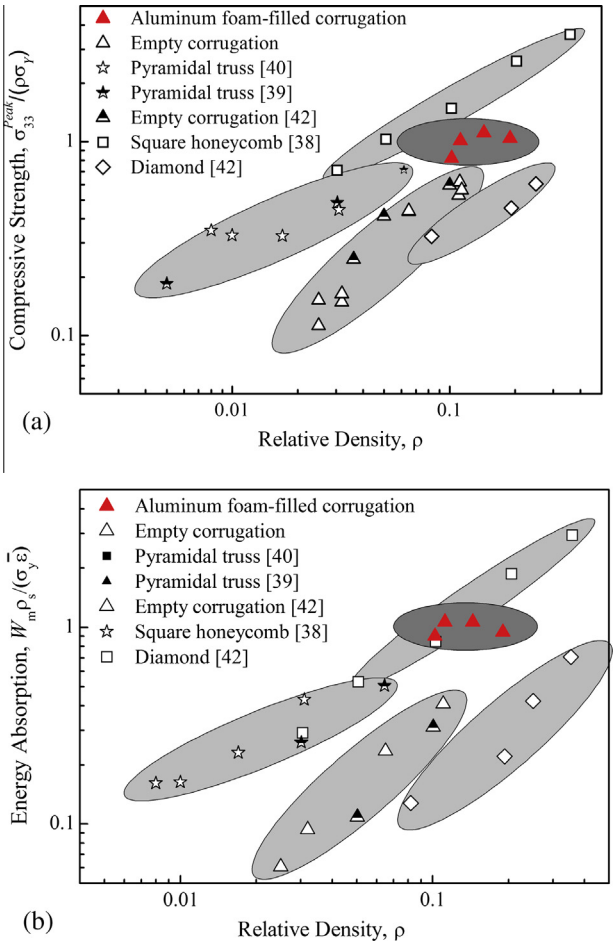

Fig. 9. Comparison of experimentally measured (a) peak compressive strength and (b) specific energy absorption of competing sandwich core designs (unless otherwise stated, test data obtained from the present study).

[1] For interpretation of color in Fig. 8, the reader is referred to the web version of this article.

compressive stress–strain curve. However, for weight sensitive applications, energy absorbers with minimum mass were critical, so SEA (absorbed energy per unit mass) was more important. The absorbed energy per unit mass, W_m, may be defined as:

$$W_m = W_V/\rho_c \tag{32}$$

where $W_V = \int_0^{\bar{\varepsilon}} \sigma d\varepsilon$ was the energy absorbed per unit volume. In the present study, the integration was up to the strain of $\bar{\varepsilon} = 0.5$.

To plot Fig. 9, the peak compressive strength and SEA of each sandwich were normalized as $\sigma_{33}^{Peak}/(\rho\sigma_Y)$ and $W_m\rho_s/(\sigma_Y\bar{\varepsilon})$, where σ_Y and ρ_s were the yield stress and density of 304 stainless steel, and $\rho = \rho_c/\rho_s$ was the average relative density of the sandwich core.

The results of Fig. 9 demonstrated that the compressive strength and specific energy absorption of the aluminum foam-filled corrugated core were considerably more competitive than empty corrugated, diamond and pyramidal truss cores, and comparable with the square-honeycomb core. Further, given the ineluctable defects during vacuum brazing and fabrication cost of square-honeycomb and pyramidal truss cores, the defect-insensitive foam-filled corrugated core became even more advantageous. It had also been established that, compared with empty corrugated cores having the same relative density, the aluminum foam-filled corrugated cores resulted in significant increase of peak compressive strength and energy absorption capacity. The significant increase of the peak stress and SAE was contributed to the sufficient lateral support to the corrugated core member supplied by the filling aluminum foam, altering not only the deformation modes but also delaying considerably core member buckling [1]. In contrast, whilst the filling of polyurethane foams into hexagonal aluminum honeycombs increased substantially the mean crushing strength and energy absorption capacity, it did not lead to enhanced SAE [41]. In addition, to increase the mean crushing strength and energy absorption of hexagonal cell aluminum honeycombs [41] and thin walled sections [42], increasing simply the wall thickness was proved to be more effective than filling with polyurethane foams.

7. Conclusions

Sandwich beams with aluminum foam-filled corrugated cores were fabricated and experimentally studied under three-point bending. The bending stiffness, initial failure load and peak load of the sandwich structure were all predicted by theoretical analysis. The analytical predictions agreed well with those experimentally measured. Relative to an unfilled corrugated sandwich, the filling of aluminum foams led to dramatically increased bending stiffness, initial failure load, peak load, and sustained load-carrying capacity after peak failure. This was accompanied by observed distinct changes in failure mechanisms, from elastic face wrinkling and elastic core buckling to plastic face yielding/wrinkling and indentation, which matched well with those predicted. Failure mechanism maps were subsequently constructed for both empty and filled sandwich beams. With outstanding bending performance as well as high specific compressive strength and specific energy absorption, metallic foam-filled sandwich constructions hold great potential as novel lightweight structural materials for a wide range of structural and crushing/impulsive loading applications.

Acknowledgments

This work was supported by the National Basic Research Program of China (2011CB610305), the National Natural Science Foundation of China (11021202, 11072188 and 11102152), the National 111 Project of China (B06024), the Shaanxi Province 13115 Project, and the Fundamental Research Funds for Xi'an Jiaotong University (xjj2011007).

References

[1] Yan LL, Yu B, Han B, Chen CQ, Zhang QC, Lu TJ. Compressive strength and energy absorption of sandwich panels with aluminum foam-filled corrugated cores. Compos Sci Technol 2013;86:142–8.
[2] Gibson LJ, Ashby MF. Cellular solids: structure and properties. Cambridge: Cambridge University Press; 1997.
[3] Ashby MF, Evans AG, Fleck NA, Gibson LJ, Hutchinson JW, Wadley HNG. Metal foams: a design guide. London: Butterworth/Heinemann; 2000.
[4] Wang B, Wu LZ, Ma L, Sun YG, Du SY. Mechanical behavior of the sandwich structures with carbon fiber-reinforced pyramidal lattice truss core. Mater Des 2010;31:2659–63.
[5] Kooistra GW, Wadley HN. Lattice truss structures from expanded metal sheet. Mater Des 2007;28:507–14.
[6] Fan HL, Jin FN, Fang DN. Uniaxial local buckling strength of periodic lattice composites. Mater Des 2009;30:4136–45.
[7] Yan CZ, Hao L, Hussein A, Young P, Raymont D. Advanced lightweight 316L stainless steel cellular lattice structures fabricated via selective laser melting. Mater Des 2014;55:533–41.
[8] Banhart J. Manufacture, characterisation and application of cellular metals and metal foams. Prog Mater Sci 2001;46:559–632.
[9] Schüler P, Sebastian FF, Bührig-Polaczek A, Claudia F. Deformation and failure behaviour of open cell Al foams under quasistatic and impact loading. Mat Sci Eng A-Struct 2013;587:250–61.
[10] Jeon I, Asahina T. The effect of structural defects on the compressive behavior of closed-cell Al foam. Acta Mater 2005;53:3415–23.
[11] Chen CQ, Lu TJ, Fleck NA. Effect of imperfections on the yielding of two-dimensional foams. J Mech Phys Solids 1999;47:2235–72.
[12] Vaidya UK, Ulven C, Pillay S, Ricks H. Impact damage of partially foam-filled co-injected honeycomb core sandwich composites. J Compos Mater 2003;37:611–26.
[13] Vaziri A, Xue ZY, Hutchinson JW. Metal sandwich plates with polymer foam-filled cores. J Mech Mater Struct 2006;1:97–127.
[14] Yazici M, Wright J, Bertin D, Shukla A. Experimental and numerical study of foam filled corrugated core steel sandwich structures subjected to blast loading. Compos Struct 2014;110:98–109.
[15] Yang L, Fan HL, Liu J, Ma Y, Zheng Q. Hybrid lattice-core sandwich composites designed for microwave absorption. Mater Des 2013;50:863–71.
[16] Ostos JB, Rinaldi RG, Hammetter CM, Stucky GD, Zok FW, Jacobsen AJ. Deformation stabilization of lattice structures via foam addition. Acta Mater 2012;60:6476–85.
[17] Zhang GQ, Wang B, Ma L, Wu LZ, Pan SD, Yang JS. Energy absorption and low velocity impact response of polyurethane foam filled pyramidal lattice core sandwich panels. Compos Struct 2014;108:304–10.
[18] Zhang J, Supernak P, Mueller-Alander S, Wang CH. Improving the bending strength and energy absorption of corrugated sandwich composite structure. Mater Des 2013;52:767–73.
[19] Chen DH. The collapse mechanism of corrugated cross section beams subjected to three-point bending. Thin Wall Struct 2012;51:82–6.
[20] Seong DY, Jung CG, Yang DY, Moon KJ, Ahn DG. Quasi-isotropic bending responses of metallic sandwich plates with bi-directionally corrugated cores. Mater Des 2010;31:2804–12.
[21] Rubino V, Deshpande VS, Fleck NA. The three-point bending of Y-frame and corrugated core sandwich beams. Int J Mech Sci 2010;52:485–94.
[22] Russell BP, Liu T, Fleck NA, Deshpande VS. Quasi-static three-point bending of carbon fiber sandwich beams with square honeycomb cores. J Appl Mech-T ASME 2011;78:031008.
[23] Crupi V, Epasto G, Guglielmino E. Collapse modes in aluminium honeycomb sandwich panels under bending and impact loading. Int J Impact Eng 2012;43:6–15.
[24] Xiong J, Ma L, Pan SD, Wu LZ, Papadopoulos J, Vaziri A. Shear and bending performance of carbon fiber composite sandwich panels with pyramidal truss cores. Acta Mater 2012;60:1455–66.
[25] McCormack TM, Miller R, Kesler O, Gibson LJ. Failure of sandwich beams with metallic foam cores. Int J Solids Struct 2001;38:4901–20.
[26] Zu GY, Song BN, Zhong ZY, Li XB, Mu YL, Yao GC. Static three-point bending behavior of aluminum foam sandwich. J Alloy Compd 2012;540:275–8.
[27] Styles M, Compston P, Kalyanasundaram S. The effect of core thickness on the flexural behaviour of aluminium foam sandwich structures. Compos Struct 2007;80:532–8.
[28] Steeves CA, Fleck NA. Collapse mechanisms of sandwich beams with composite faces and a foam core, loaded in three-point bending. Part II: experimental investigation and numerical modelling. Int J Mech Sci 2004;46:585–608.
[29] Marsavina L, Sadowski T, Knec M, Negru R. Non-linear behaviour of foams under static and impact three point bending. Int J Nonlin Mech 2010;45:969–75.
[30] Yu JL, Wang E, Li JR, Zheng ZJ. Static and low-velocity impact behavior of sandwich beams with closed-cell aluminum-foam core in three-point bending. Int J Impact Eng 2008;35:885–94.
[31] Qi C, Yang S, Yang LJ, Wei ZY, Lu ZH. Blast resistance and multi-objective optimization of aluminum foam-cored sandwich panels. Compos Struct 2013;105:45–57.

[32] Yang DH, Hur BY, He DP, Yang SR. Effect of decomposition properties of titanium hydride on the foaming process and pore structures of Al alloy melt foam. Mat Sci Eng A-Struct 2007;445:415–26.
[33] Han B, Zhang QC, Lu TJ. Design optimization of foam-lattice hybrid core sandwich beams in three-point bending. 2013.
[34] Allen HG. Analysis and design of structural sandwich panels. Oxford: Pergamon Press; 1969.
[35] Han B, Yan LL, Yu B, Zhang QC, Chen CQ, Lu TJ. Collapse mechanisms for metal sandwich plates with aluminum foam-filled corrugated cores 2013. under review.
[36] Chen TY, Shen SH. Buckling of structures. Shanghai: Shanghai Science and Technology Literature Press; 1993.
[37] Cote F, Deshpande VS, Fleck NA, Evans AG. The compressive and shear responses of corrugated and diamond lattice materials. Int J Solids Struct 2006;43:6220–42.
[38] Cote F, Deshpande VS, Fleck NA, Evans AG. The out-of-plane compressive behavior of metallic honeycombs. Mat Sci Eng A-Struct 2004;380:272–80.
[39] Zok FW, Waltner SA, Wei Z, Rathbun HJ, McMeeking RM, Evans AG. A protocol for characterizing the structural performance of metallic sandwich panels: application to pyramidal truss cores. Int J Solids Struct 2004;41:6249–71.
[40] Zhang QC, Han YJ, Chen CQ, Lu TJ. Ultralight X-type lattice sandwich structure (I): concept, fabrication and experimental characterization. Sci China, Ser E 2009;39:1039–46.
[41] Nia AA, Sadeghi MZ. The effects of foam filling on compressive response of hexagonal cell aluminum honeycombs under axial loading-experimental study. Mater Des 2010;31:1216–30.
[42] Chen WG, Wierzbicki T. Relative merits of single-cell, multi-cell and foam-filled thin-walled structures in energy absorption. Thin Wall Struct 2001;39:287–306.